Atmos. Chem. Phys. Discuss., 10, 29971–29995, 2010
www.atmos-chem-phys-discuss.net/10/29971/2010/
doi:10.5194/acpd-10-29971-2010


Atmospheric Chemistry and Physics Discussions



# Enhancements of gravity wave amplitudes at midlatitudes during sudden stratospheric warmings in 2008

**T. Flury**[1,3], **K. Hocke**[1,2], **N. Kämpfer**[1,2], **and D. L. Wu**[3]

[1]Institute of Applied Physics, University of Bern, Sidlerstrasse 5, 3012 Bern, Switzerland
[2]Oeschger Centre for Climate Change Research, University of Bern, Bern, Switzerland
[3]Jet Propulsion Laboratory, California Institute of Technology, Pasadena, California, USA

Received: 12 August 2010 – Accepted: 28 November 2010 – Published: 9 December 2010

Correspondence to: T. Flury (thomas.flury@jpl.nasa.gov)

Published by Copernicus Publications on behalf of the European Geosciences Union.







## Abstract

Two minor and one major stratospheric warming happened in January and February 2008 when the polar vortex was shifted toward midlatitudes. The analysis of temperature profiles from radiosondes in Payerne (Switzerland) during this period reveals an enhancement of gravity wave amplitudes between 25 and 30 km altitude especially during the two minor warmings around 20 January and 1 February. Increases of gravity wave amplitudes in the mid-stratosphere are associated with a strong tropopause jet and the presence of the polar vortex edge over Switzerland.

## 1 Introduction

Atmospheric gravity waves (GW) play an important role for the dynamics of the middle atmosphere. Gravity waves can be generated in the troposphere by airflow over mountains or by convection of moist air. Further GW can be produced by spontaneous radiation in wind shear associated with the tropopause jet or the polar night jet in the stratosphere (Plougonven et al., 2003). GW transport momentum over long distances and deposit their momentum in the mean atmospheric flow through dissipation or breaking processes. The latter leads to a global scale meridional circulation in the mesosphere driven by gravity waves with rising motion over the summer pole, transport and descent toward and over the winter pole. As a surprising consequence, the coldest point in the atmosphere is found at the summer polar mesopause (Shepherd, 2000). A review of GW is given by Fritts and Alexander (2003). The propagation of GW from the troposphere to the middle atmosphere depends on the wind regimes. GW can be filtered by so called critical levels where the background wind matches the phase speed of the wave. An interesting situation for GW is given during so called sudden stratospheric warmings SSW, during which the wind in the middle atmosphere is particularly variable with strong wind shears. SSWs are dynamical events which occur frequently in winter at mid- to high-northern latitudes. They are characterized by a





ACPD

10, 29971–29995, 2010



sudden increase in temperature and a deceleration or even reversal of the prevailing zonal eastward wind. SSWs happen when the eastward mean flow of the polar stratosphere interacts with planetary waves originating in the troposphere (Matsuno, 1971). SSW lead to a displacement or even break up of the polar vortex. GW may also play a role in forcing of SSWs when propagating into the stratosphere as a consequence of variations of the tropopause jet during instabilities in the upper troposphere.

Flury et al. (2009) detected pronounced wind shears during three SSW in 2008 when the polar vortex edge was above Switzerland motivating the investigation of GW in the disturbed wind field during the SSW. In contrast to midlatitudes there exist several highlatitude studies about enhanced gravity wave activity during SSW and at the polar vortex edge. Ratnam et al. (2004) investigated the GW activity during the exceptional southern hemisphere SSW in September 2002 by using CHAMP/GPS radio occultation temperature profiles. They concluded that GW activity was enhanced during the warming especially near the edge of the splitted polar vortex. Baumgaertner and McDonald (2007) present a GW climatology for Antarctica using the same CHAMP/GPS satellite observations and also found an increase of GW activity at the polar vortex edge. More recent radio occultation measurements are available from the COSMIC-FORMOSAT-3 experiment (Liou et al., 2007). Whiteway et al. (1997) investigated gravity waves in temperature fluctuations measured by LIDAR at Eureka station (80° N, 86° W) and found maximal wave activity when the station was beneath the polar vortex edge and minimal inside the vortex. Baumgaertner and McDonald (2007) and Whiteway et al. (1997) attributed the enhanced wave activity to reduced critical level filtering. Another mechanism leading to enhanced gravity wave amplitudes was pointed out by Yoshiki and Sato (2000). The observed enhancement of gravity wave amplitudes seen in radiosonde temperatures above the Arctic winter and Antarctic spring was attributed to waves directly generated at the stratospheric vortex edge. Wang and Alexander (2009) investigated gravity waves for the SSW of 2008. They used high resolution temperature profiles of HIRDLS (High Resolution Dynamics Limb Sounder) on the Aura satellite and found larger GW amplitudes at the vortex edge and smaller in the vortex core and





ACPD
10, 29971–29995, 2010



outside of the vortex. They assumed a higher transmission of waves from the troposphere into the stratosphere at the vortex edge due to the strong jet winds.

We investigate the gravity wave amplitudes at midlatitudes in Switzerland during two minor SSW in the beginning of 2008. Gravity waves above the Alps during a SSW are poorly investigated yet, hence we try to shed light on it and utilize in situ measurements of radiosondes inside-, outside- and at the edge of the polar vortex. The radiosonde measurements are expected to provide information about GW activity on horizontal scales which are invisible for satellites. Fritts et al. (2006) argue that GW with high intrinsic frequencies and small amplitudes have large energy and momentum fluxes and atmospheric effects. The article is organized as follows. In Sect. 2 we describe the method used to define a gravity wave amplitude. In Sect. 3 we discuss the results and the link of gravity waves with the polar vortex and the tropopause jet.

## 2 Data analysis

We extract gravity waves from temperature and wind profiles. The data are taken from the radiosondes launched at 12:00 UTC and 00:00 UTC from the midlatitude MeteoSwiss station in Payerne (46.8° N, 6.9° E, 491 m a.s.l.). The temperature is recorded with the Swiss sonde SRS 400 with an accuracy of 0.1 K and with a time resolution of between 1 and 3 s (Richner, 1999). The balloons reach an altitude of typically 34 km. Then we use satellite data from the AMSU-A instrument on the NASA Aqua spacecraft to get an overview of GWs above Europe. Fluctuations in measured microwave radiances at 60 GHz trace the GW field (Wu et al., 2006). Finally ECMWF (European Centre for Medium range Weather Forecast) reanalysis data are taken for wind and vorticity studies in connection with the polar vortex.

Daily radiosonde temperature profiles from the period from 1 January to 23 February 2008 are taken. These are in total about 109 profiles which are displayed in Fig. 1. For the study of stratospheric GW we concentrate on the height range 13 to 32 km to eliminate the influence of the sharp temperature change at the tropopause in the used digital filter.





ACPD
10, 29971–29995, 2010



A gravity wave produces periodic fluctuations in the temperature profile $T(t)$, where $t$ is the flight time of the balloon. These fluctuations can be evaluated with respect to their periods by using a bandpass function applied on the measured temperature profile. Every profile (time series of balloon ascent) is filtered for periods $T_p$ between 150 s and 500 s with a time step of 10 s and a bandpass width of $\frac{T_p}{5}$. In this way a bandpass filtered series $S_{T_p}(t)$ is obtained for every period. The amplitude $a_{T_p}(t)$ of an oscillation with the period $T_p$ is derived as a function of time from the bandpass filtered series $S_{T_p}(t)$ according to Eq. (1) (Hocke, 2009)

$$a_{T_p}(t) = \frac{\pi}{2T_p} \int_{t-T_p/2}^{t+T_p/2} \left| S_{T_p}(t') \right| dt' . \quad (1)$$

The resulting amplitude series $a_{T_p}(t)$ can also be expressed as a function of altitude $z$ which is measured by a GPS receiver on the balloon. This yields an amplitude height profile $a_{T_p}(z)$, which will be used later in the results. Additionally the period $T_p$ can be translated into a vertical wavelength $\lambda_z$ if horizontal and temporal variations of the GW during the flight are neglected. Since the orography of Switzerland is dominated by many mountains with small horizontal spacing, we hesitate to do the neglection. Instead we provide both, information on $T_p$ and $\lambda_z$. For every single radiosonde profile the average of all amplitudes $a_{T_p}(t)$ calculated by Eq. (1) for the periods $T_p = 250$ s, 260 s, 270 s,···, 500 s is taken as the mean gravity wave amplitude. The choice of the periods $T_p \in [250;500]$ s or $\lambda_z \in [1.6;3.3]$ km, assuming a balloon ascent speed of 6.5 m s$^{-1}$, comprises high-frequency gravity waves as well as inertia gravity waves, depending on the interpretation of the spatio-temporal fluctuations along the radiosonde trajectory.

## 3 Results

Figure 1 shows single temperature profiles equidistantly shifted by 7 K along the x-axis and chronologically ordered from 1 January to 23 February. The red profiles were





ACPD
10, 29971–29995, 2010



measured during the minor SSWs of 18 to 22 January and 31 January to 7 February showing clear disturbances at altitudes above 25 km, a region which is affected by the polar vortex, which was shifted to Switzerland in these SSW periods. We will refer to these two time periods as "active time periods". During the major SSW from 17 to 23 February (last 14 profiles), the profiles are not particularly disturbed on small scales, but the temperatures decreased to 190 K at 20 km and increased to 295 K above 30 km (see Flury et al., 2009, for a detailed discussion), while Switzerland was clearly inside the polar vortex, see Fig. 7. The gravity wave analysis of the temperature profiles will follow later in Sect. 3.3.

### 3.1 Orographic gravity waves

Orographic gravity waves are produced by airflow over mountains. Doyle and Smith (2003) showed that waves with short horizontal wavelengths of 10 to 20 km are produced by airflow over the Alps in the troposphere. Such gravity waves can also penetrate and propagate into the stratosphere which was simulated and observed by Schoeberl (1985) and Smith et al. (2008) respectively. Figure 2a shows that all the balloons launched in Payerne during the active time period (18–21 January 2008) flew over the Swiss Alps. The trajectories go in south-eastern direction over the Alps which are in the south of the oblique black line in Fig. 2a. Hence we would expect signs of orographic gravity waves in the soundings. Indeed a closer inspection in a balloon's trajectory plotted in Fig. 2b shows periodic disturbations in the stratosphere caused by orographic gravity waves. This 3 dimensional trajectory is from the radiosonde launched at noon on 21 January 2008. The x and y coordinates are given in degrees latitude and longitude. The start of the trajectory is in Payerne (46.8° N, 6.9° E, 491 m a.s.l.). The balloon flew up to an altitude of about 30 km over the Swiss Alps (this trajectory corresponds to the blue line in Fig. 2a. The topography below the balloon is plotted in red (heights multiplied by a factor of 3 for a better visualization). A wavelike feature is visible on small scales between 15 and 30 km altitude, the same altitude range where the temperature profile is disturbed (Fig. 1). The vertical distance between the bumps





ACPD
10, 29971–29995, 2010



is approximately 2.5 km and 20 km in horizontal distance. The vertical distance corresponds to the usually observed vertical wavelength of long-period gravity waves in the mid-stratosphere (Schöllhammer, 2002). On the other hand the disturbed balloon trajectory could also be explained by high-frequency gravity waves of small horizontal scales which is for instance not visible for a satellite. It is likely that high-frequency GW and inertia GW occur at the same time. Figure 3 however supports the assumption for high-frequency orographic gravity waves observed here. It shows on the left the temperature and on the right the balloon ascent rate of the sounding of 21 January 23:00. The temperature profile shows a wave signal with an amplitude of about 2.5 K and an apparent vertical wavelength $\lambda_z^*$ of 2 to 2.5 km. The variation of the balloon ascent rate is quite strong with amplitudes of about 1 m s$^{-1}$, which is indicative for short period (high frequency) orographic GW since high values of vertical wind perturbations can be excluded for long-period waves (Sato et al., 1997) whereas they are typical for short-period mountain waves (Kitchen and Shutts, 1990; Romanens and Jacquemin, 2007). Notice however that the apparent vertical wavelength in the ascent rate of 1.5 to 2 km is shorter than in the temperature data. The different apparent wavelengths in the same sounding suggest that simple linear wave theory fails here.

We find that the temperature and the ascent rate are close to an anticorrelation between 23 and 28 km altitude (shaded in Fig. 3, blue = cooling, red = warming). However linear wave theory would suggest a quadrature relationship (phase shift of 90°) between both quantities, which was observed in another radiosounding study led at Payerne by Romanens and Jacquemin (2007). In this particular sounding here, we do not observe it. This may be due to a superposition of different waves or happen in a heavily damped system, where the temperature anomaly can be forced to occur very soon after the ascent rate anomaly (T. Dunkerton, personal communication, 2010). However the anticorrelation is not so far away from the expected 90° phase shift which can be explained by the theory of adiabatic heating and cooling. The temperature decreases whilst the ascent rate increases, which is a sign of upward vertical motion, which accelerates the balloon and cools the air adiabatically. When the ascent rate





ACPD
10, 29971–29995, 2010



slows down, which is indicative for downward motion, the air heats up. However this simple correspondence is not given over the whole altitude range. We hope to get some clues in the discussion of this article

Figure 4 illustrates the sampling issue of radiosonde data. Kitchen and Shutts (1990) showed the difficult way how to extract orographic gravity waves with sloping phase fronts from radiosonde data. The derived frequencies were near to the Brunt-Vaisala frequency and horizontal wavelengths were around 10 km. We find the same here by assuming wave fronts as up- and downdrafts as shown in Fig. 4 with a vertical wavelength $\lambda_z = \infty$ and a horizontal wavelength $\lambda_h$. With the vertical speed $v_{asc}$ of the balloon (ascent rate) and the apparent vertical wavelength $\lambda_z^*$, which we take from the sounding displayed in Fig. 3, ($\lambda_z^* = 2$ km, $v_{asc} = 6.5\,\mathrm{m\,s^{-1}}$ in the given example) we can calculate the wave period $T$ as well as the horizontal wavelength $\lambda_h$ since we know the horizontal speed $u_h = \|\boldsymbol{u}\| = \sqrt{u^2 + v^2}$ of the balloon ($u_h = 38\,\mathrm{m\,s^{-1}}$ is the mean horizontal wind over the altitude range 20 to 30 km in the given example). We get the following

$$T = \frac{\lambda_z^*}{v_{asc}} = \frac{2000\ \mathrm{m}}{6.5\ \mathrm{m\,s^{-1}}} = 307\ \mathrm{s} \qquad \lambda_h = T \cdot u_h = 307\ \mathrm{s} \cdot 38\ \mathrm{m\,s^{-1}} = 11.67\ \mathrm{km} \tag{2}$$

These are quite realistic values for local mountain waves which are often observed over the Swiss Alps. The intrinsic wave period $T = 307$ s = 5.1 min is close to the Brunt-Vaisala period, which is also typical for a high-frequency orographic gravity wave (Kitchen and Shutts, 1990). The interpretation is further supported by the large vertical wind perturbation observed by the balloon and shown in Fig. 3. This scheme however shows that one needs to be careful with the interpretation of observed vertical wavelengths.

### 3.2 Inertia gravity waves

Sudden stratospheric warmings are not only accompanied by orographic gravity waves but also by inertia gravity waves with much longer horizontal wavelengths (Wang and





ACPD
10, 29971–29995, 2010



Alexander, 2009). Eckermann et al. (2006) observed that small-scale GW with $\lambda_h$ of 10–20 km be superposed on medium-scale GW with $\lambda_h$ of 100–200 km leading to the formation of polar stratospheric clouds in Arctic regions for instance. Satellites can observe such medium- and large-scale GW with horizontal wavelengths of hundreds of kilometers. Figure 5 shows AMSU radiances at 2 different altitudes, channel 13 corresponds to 5 hPa (~34 km) and channel 9 to 80 hPa (~18 km). The left figure shows radiances on 21 January 2008 at 5 hPa. A wave field from France to Scandinavia is visible with a horizontal wavelength of about 550 km, Switzerland lies also beneath it. The wave field on 22 January 2008 at 80 hPa is shown on the right. The wavelength is about 450 km and the propagation is north-south from Germany to northern Italy across the Swiss Alps. Figure 6 shows the ECMWF modified potential vorticity (Lait, 1994) and wind field corresponding to the time and location of the two AMSU figures (Fig. 5). One can see that the wind direction is perpendicular to the wave fronts. The figure on the left at 34 km altitude displays that the location of the vortex edge (orange to red areas over Scandinavia) corresponds well with the location of the wave field. On the right the wind direction changes after passing through the gravity wave field.

### 3.3 Gravity wave amplitudes

A more rigorous search for gravity waves according to the method explained in Sect. 2 leads to the top panel of Fig. 7. It shows the gravity wave amplitude averaged for wave periods between 250 s and 500 s, where the interval includes at the lower boundary the usual Brunt-Vaisala period in the stratosphere. There are high amplitudes around 20 km altitude on 6 and 7 January as well as on 22 January and 7 February. Longer time periods with high GW amplitudes are found at 25 to 30 km altitude from 17 January to 22 January as well as from 31 January to 5 February. These periods correspond to the time of the two minor sudden stratospheric warmings (SSW) (Flury et al., 2009). We did not observe enhanced GW amplitudes during the major SSW from 17 February to 23 February. Hence we can not simply conclude that SSWs are positively correlated to gravity wave amplitudes. There needs to be another explanation which will follow.





ACPD
10, 29971–29995, 2010



### 3.4 Polar vortex

Considering atmospheric oscillations we notice that the Brunt-Vaisala frequency $N$ depends on the static stability of the atmosphere and is computed by the formula

$$N^2 = \frac{g}{\theta}\frac{\partial\theta}{\partial z} \tag{3}$$

where $g$ is the Earth acceleration, $\theta$ is potential temperature and $z$ the vertical coordinate.

The polar vortex is characterized by high potential vorticity PV, which is defined by (Ertel's potential vorticity)

$$\mathrm{PV} = -(\xi + f)g\frac{\partial\theta}{\partial p} \tag{4}$$

Where $\xi = \frac{\partial v}{\partial x} - \frac{\partial u}{\partial y}$ is the relative vorticity with zonal and meridional wind speed $u$ and $v$, $f = 2\Omega\sin\Phi$ is the Coriolis parameter with $\Omega$ the Earth's rotation rate and $\Phi$ latitude and $p$ is atmospheric pressure, which is a function of the height $z$. Both quantities depend on the static stability $\frac{\partial\theta}{\partial z}$ resp. $-\frac{\partial\theta}{\partial p}$. The Brunt-Vaisala frequency $N$ is the limiting upper frequency for gravity waves and PV is the quantity for the characterization of the polar vortex. This link between gravity waves and the potential vorticity and the work done by Baumgaertner and McDonald (2007); Ratnam et al. (2004); Yoshiki and Sato (2000) leads us to the analysis of the polar vortex during the stratospheric warming and its possible involvement in the increased GW amplitudes.

The lower panel of Fig. 7 shows the time height series of ECMWF modified potential vorticity (Lait PV, Lait, 1994) for Payerne. If we compare this figure to the measured gravity wave amplitudes in the upper panel we notice, that the correspondence is given for the days around 20 January and 1 February, but there is little correspondence during the major SSW period around 20 February. The difference of the 3 high vorticity periods is that the last one shows much higher vorticity values, suggesting that the column of air above Payerne was clearly inside the polar vortex whereas in the other





ACPD
10, 29971–29995, 2010



two cases Payerne was at the edge of the vortex. This fact is better shown in the middle panel of Fig. 7, which shows the latitudinal dependence of potential vorticity along the Payerne Meridian of 7° E. The white dashed line shows the latitude of Payerne. We define the vortex edge as the light green color (~2.5 Lait PV units), where there is a clear meridional gradient, and observe that the enhanced gravity wave amplitudes measured by the radiosondes correlate well with Payerne being at the vortex edge. We conclude that higher GW amplitudes are observed at the edge of the polar vortex rather than inside.

As already stated in studies for polar latitudes (Yoshiki and Sato, 2000; Baumgaertner and McDonald, 2007) increased gravity wave amplitudes are linked to the polar vortex edge during a stratospheric warming. We even observe it here at midlatitudes. One could imagine the vortex as a rigid rotor which is pushed out of equilibrium and then the axis of rotation begins to precess. The edge of the vortex shows the strongest shear flow, which is balanced by spontaneous emission of gravity waves (Williams et al., 2003).

### 3.5 Tropopause jet

Figure 8 merges the radiosonde gravity wave amplitudes (contours), the same as shown in Fig. 7, with the measured horizontal wind speed. Pulsations of the strength of the tropopause jet are obvious in Fig. 8. There is a connection of the tropopause jet and the wave amplitudes in the lower stratosphere and between 25 and 30 km. The strong tropopause jet could lead to enhanced gravity wave radiation into the lower stratosphere. The GW from below can propagate higher up when the polar vortex is present. This connection was already observed by Pavelin et al. (2001) and Plougonven et al. (2003). They related the higher wave amplitudes with highly curved jet streams and planetary wave breaking. The presence of a curved tropopause jet is always linked with the presence of gravity waves, while the curvature of the tropopause jet can be caused by a blocking or a planetary wave. Thus gravity waves are a possible link between





ACPD
10, 29971–29995, 2010



tropospheric blockings and SSWs. Martius et al. (2009) found a strong correlation between blockings and SSWs.

### 3.6 Wave characteristics

In order to demonstrate which wave periods (or vertical wavelengths) were particularly enhanced during the minor warmings we filtered the profiles for periods between 150 s and 500 s as explained in Sect. 2 and calculated a temporal average for the active period (minor SSW, 18–23 January) and for the quiet time of 23–30 January. The relative difference (active minus quiet divided by quiet) is shown in Fig. 9. Especially the amplitudes of the waves with periods between 250 s and 350 s from 26 to 30 km altitude are increased by a factor of 4. The period range is conform with the Brunt-Vaisala period of the stratosphere. On the other hand, assuming a balloon ascent speed of 6.5 m s$^{-1}$, the periods would correspond to vertical wavelengths $\lambda_z$ of 1.6 km to 3.2 km, typical for long-period GW. The amplitudes remain increased up to periods of 500 s which is the reason we chose the interval from 250 to 500 s for the definition of the mean GW amplitude. In the lower stratosphere at 13 to 25 m there was also a general increase for all the periods analyzed but less pronounced.

## 4 Conclusions

In January and February 2008 two minor and one major sudden stratospheric warming occurred and the polar vortex was shifted south toward Switzerland. During the two minor sudden stratospheric warmings from 18 to 23 January and 31 January to 5 February Switzerland was at the polar vortex edge. The major sudden stratospheric warming of 20 February shifted the polar vortex even further south so that Switzerland was clearly inside the vortex. The analysis of temperature profiles of radiosondes showed that the gravity wave activity was clearly enhanced during the minor sudden stratospheric warmings. The reason for this is assumed to be an interplay of the





ACPD
10, 29971–29995, 2010



tropospheric jet stream, upward gravity wave flux and the displacement of the polar vortex to Switzerland. Gravity wave amplitudes between 25 and 30 km altitude are larger at the vortex edge than inside and outside of the vortex, an observation which is supported by the study of Wang and Alexander (2009). During days with a strong tropopause jet over Switzerland, the gravity wave amplitudes were increased also in the lower stratosphere suggesting the tropopause jet as the source of gravity wave radiation. Satellite images of AMSU reveal a detailed picture of the gravity wave field above Europe and its relation to the polar vortex. We assume that the radiosondes observed a superposition of inertia gravity waves and high-frequency orographic gravity waves during the sudden stratospheric warming events. Hence a combination of in situ radiosonde measurements and satellite images can improve the interpretation of gravity wave observations.

*Acknowledgements.* This work has been supported by the Swiss National Science Foundation under grants Nr. 200020-124387/1 and Nr. 00021_124414. It has partly been elaborated during the workshop "Bridging the gap between the middle and upper atmosphere: coupling processes due to winds and waves over an extended altitude range" sponsored by the International Space Science Institute (ISSI) located at Bern. Thanks to MeteoSwiss Payerne, ECMWF and NASA for the meteorological data. One of the authors (KH) was supported by the Oeschger Centre for Climate Change Research (OCCR). Thanks to the editor for useful advices and comments during the preparation of this manuscript.





ACPD
10, 29971–29995, 2010



## References


Baumgaertner, A. J. G. and McDonald, A. J.: A gravity wave climatology for Antarctica compiled from Challenging Minisatellite Payload/Global Positioning System (CHAMP/GPS) radio occultations, J. Geophys. Res., 112, 5103, doi:10.1029/2006JD007504, 2007. 29973, 29980, 29981

Doyle, J. D. and Smith, R. B.: Mountain waves over the Hohe Tauern: Influence of upstream diabatic effects, Q. J. Roy. Meteorol. Soc., 129, 799–823, doi:10.1256/qj.01.205, 2003. 29976

Eckermann, S. D., Dornbrack, A., Vosper, S. B., Flentje, H., Mahoney, M. J., Bui, T. P., and Carslaw, K. S.: Mountain wave-induced polar stratospheric cloud forecasts for aircraft science flights during SOLVE/THESEO 2000, Weather and Forecasting, 21, 42–68, 2006. 29979

Flury, T., Hocke, K., Haefele, A., Kämpfer, N., and Lehmann, R.: Ozone depletion, water vapor increase, and PSC generation at midlatitudes by the 2008 major stratospheric warming, J. Geophys. Res., 114, 18302, doi:10.1029/2009JD011940, 2009. 29973, 29976, 29979

Fritts, D. C. and Alexander, M. J.: Gravity wave dynamics and effects in the middle atmosphere, Reviews of Geophysics, 41, doi:10.1029/2001RG000106, 2003. 29972

Fritts, D. C., Vadas, S. L., Wan, K., and Werne, J. A.: Mean and variable forcing of the middle atmosphere by gravity waves, J. Atmos. Solar Terr. Phys., 68, 247–265, doi:10.1016/j.jastp.2005.04.010, 2006. 29974

Hocke, K.: QBO in solar wind speed and its relation to ENSO, J. Atmos. Solar Terr. Phys., 71, 216–220, doi:10.1016/j.jastp.2008.11.017, 2009. 29975

Kitchen, M. and Shutts, G. J.: Radiosonde observations of large-amplitude gravity waves in the lower and middle stratosphere, J. Geophys. Res., 95, 20451–20455, doi:10.1029/JD095iD12p20451, 1990. 29977, 29978

Lait, L. R.: An Alternative Form for Potential Vorticity, J. Atmos. Sci., 51, 1754–1759, doi:10.1175/1520-0469(1994)051, 1994. 29979, 29980

Liou, Y. A., Pavelyev, A. G., Liu, S. F., Pavelyev, A. A., Yen, N., Fluang, C. Y., and Fong, C. J.: FORMOSAT-3/COSMIC GPS Radio Occultation Mission: Preliminary Results, IEEE Transactions on Geoscience and Remote Sensing, 45, 3813–3826, 2007. 29973

Martius, O., Polvani, L. M., and Davies, H. C.: Blocking precursors to stratospheric sudden warming events, Geophys. Res. Lett., 36, L14806, doi:10.1029/2009GL038776, 2009. 29982

Matsuno, T.: A Dynamical Model of the Stratospheric Sudden Warming, J. Atmos. Sci., 28,






ACPD
10, 29971–29995, 2010



1479–1494, doi:10.1175/1520-0469(1971)028, 1971. 29973
Pavelin, E., Whiteway, J. A., and Vaughan, G.: Observation of gravity wave generation and breaking in the lowermost stratosphere, J. Geophys. Res., 106, 5173–5180, doi:10.1029/2000JD900480, 2001. 29981
Plougonven, R., Teitelbaum, H., and Zeitlin, V.: Inertia gravity wave generation by the tropospheric midlatitude jet as given by the Fronts and Atlantic Storm-Track Experiment radio soundings, J. Geophys. Res., 108, 4686, doi:10.1029/2003JD003535, 2003. 29972, 29981
Ratnam, M. V., Tsuda, T., Jacobi, C., and Aoyama, Y.: Enhancement of gravity wave activity observed during a major Southern Hemisphere stratospheric warming by CHAMP/GPS measurements, Geophys. Res. Lett., 31, L16101, doi:10.1029/2004GL019789, 2004. 29973, 29980
Richner, H.: Grundlagen aerologischer Messungen speziell mittels der Schweizer Sonde SRS 400, Veröffentlichungen der SMA-MeteoSchweiz 61, MeteoSchweiz, 1999. 29974
Romanens, G. and Jacquemin, D.: Analyse de qualite des mesures de radiosondage, Internal document, MeteoSwiss Payerne, p. 15, 2007. 29977
Sato, K., OSullivan, D. J., and Dunkerton, T. J.: Low-frequency inertia-gravity waves in the stratosphere revealed by three-week continuous observation with the MU radar, Geophys. Res. Lett., 24, 1739–1742, 1997. 29977
Schoeberl, M. R.: The Penetration of Mountain Waves into the Middle Atmosphere, J. Atmos. Sci., 42, 2856–2864, doi:10.1175/1520-0469(1985)042⟨2856:TPOMWI⟩2.0.CO;2, 1985. 29976
Schöllhammer, K.: Klimatologie der Schwerewellenaktivität in den mittleren Breiten, PhD thesis, Freie Universität Berlin, Berlin, Deutschland, 2002. 29977
Shepherd, T. G.: The middle atmosphere, Journal of Atmospheric and Solar-Terrestrial Physics, 62, 1587–1601, 2000. 29972
Smith, R. B., Woods, B. K., Jensen, J., Cooper, W. A., Doyle, J. D., Jiang, Q., and Grubisic, V.: Mountain Waves Entering the Stratosphere, J. Atmos. Sci., 65, 2543–2562, doi:10.1175/2007JAS2598.1, 2008. 29976
Wang, L. and Alexander, M. J.: Gravity wave activity during stratospheric sudden warmings in the 2007–2008 Northern Hemisphere winter, J. Geophys. Res., 114, 18108, doi:10.1029/2009JD011867, 2009. 29973, 29978, 29983
Whiteway, J. A., Duck, T. J., Donovan, D. P., Bird, J. C., Pal, S. R., and Carswell, A. I.: Measurements of gravity wave activity within and around the Arctic stratospheric vortex, Geophys.





ACPD
10, 29971–29995, 2010



Res. Lett., 24, 1387–1390, doi:10.1029/97GL01322, 1997. 29973
Williams, P. D., Read, P. L., and Haine, T. W. N.: Spontaneous generation and impact of inertia-gravity waves in a stratified, two-layer shear flow, Geophys. Res. Lett., 30, 2255, doi:10.1029/2003GL018498, 2003. 29981
Wu, D. L., Preusse, P., Eckermann, S. D., Jiang, J. H., Juarez, M. D. L. T., Coy, L., and Wang, D. Y.: Remote sounding of atmospheric gravity waves with satellite limb and nadir techniques, Adv. Space Res., 37, 2269–2277, doi:10.1016/j.asr.2005.07.031, 2006. 29974
Yoshiki, M. and Sato, K.: A statistical study of gravity waves in the polar regions based on operational radiosonde data, J. Geophys. Res., 105, 17995–18012, doi:10.1029/2000JD900204, 2000. 29973, 29980, 29981





ACPD
10, 29971–29995, 2010



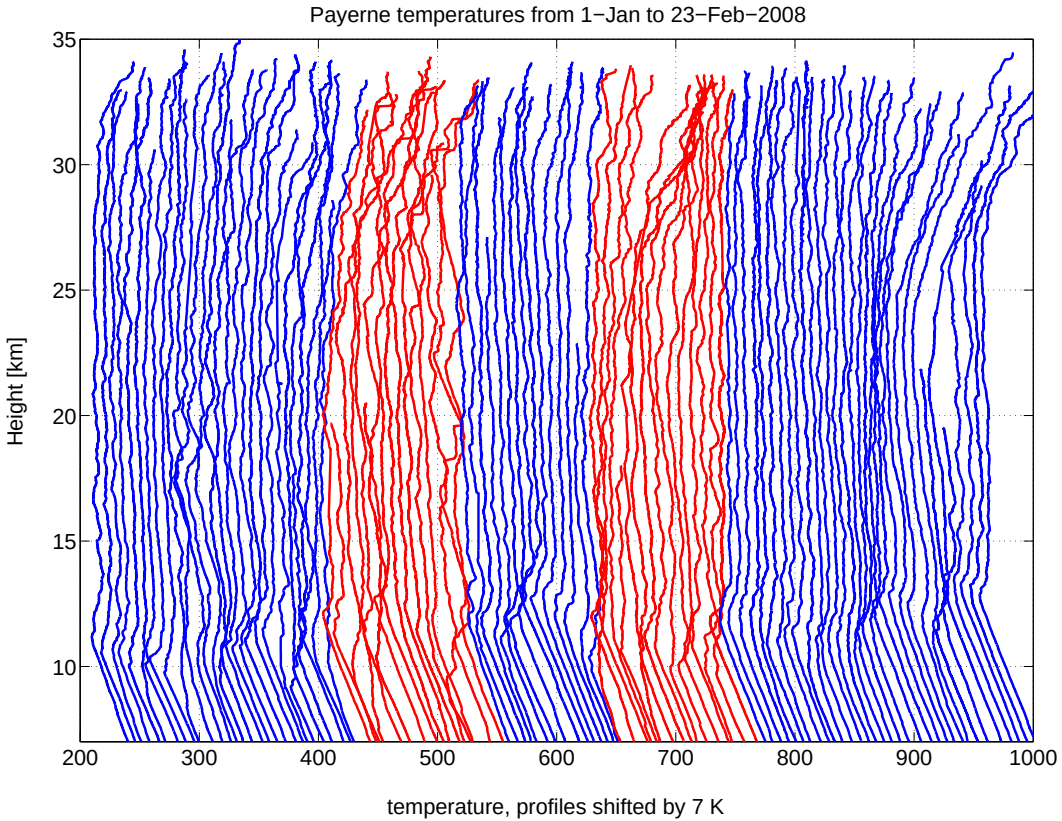


**Fig. 1.** Temperature profiles measured by radiosondes between 1 January and 23 February 2008 at Payerne Switzerland. Profiles are equidistantly shifted by 7 K. The two minor SSW periods are visualized with the red profiles which show higher wave activity (fluctuations).





ACPD
10, 29971–29995, 2010



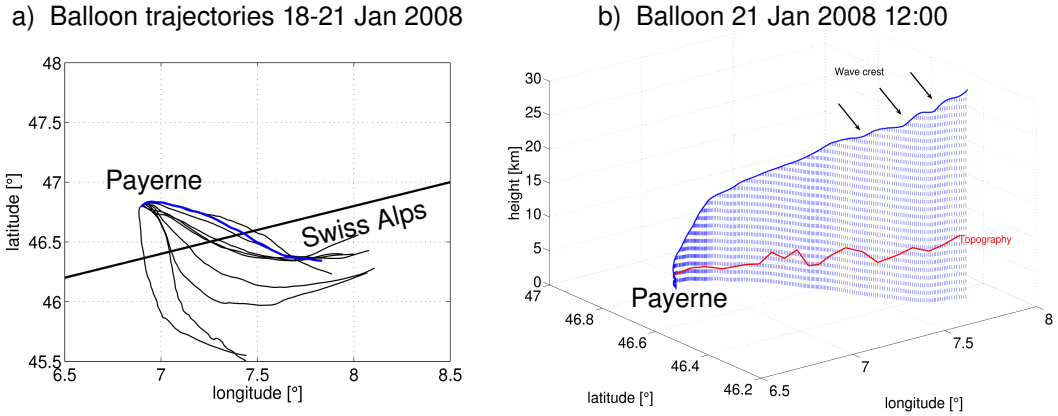


**Fig. 2. (a)** 2-D balloon trajectories during the gravity wave active time period from 18 to 21 January launched in Payerne. The balloons all went over the Swiss Alps which are south of the oblique line. The blue trajectory is also plotted in 3-D in **(b)**. **(b)** Trajectory of the balloon starting in Payerne on 21 January 2008 12:00. Blue dashed lines serve as visual help for the projected path. The wave crests beyond 15 km altitude have a vertical distance of 2.5 km and 20 km in horizontal direction. During this time the balloon flew over the Swiss Alps, which is shown by the red topography curve (for a better visualization heights of topography were multiplied by a factor of 3, maximum height 3.1 km a.s.l.).





ACPD
10, 29971–29995, 2010

High gravity wave amplitudes during SSW

T. Flury et al.



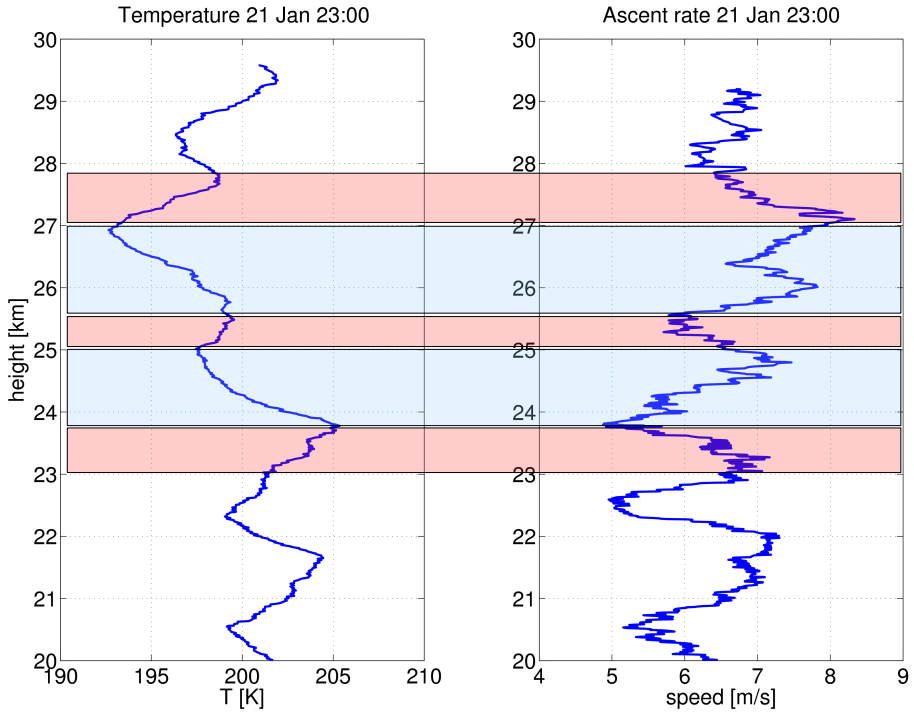


**Fig. 3.** Temperature ($T$) on the left and ascent rate ($v_{asc}$) on the right of the 21 January 23:00 sounding between 20 and 30 km altitude. The T-profile shows an apparent vertical wavelength $\lambda_z^*$ of 2 to 2.5 km whilst $v_{asc}$ has a shorter $\lambda_z^*$ of 1.5 to 2 km. Altitude ranges of a close anticorrelation are marked with red (warming) and blue (cooling). Downdrafts slow the balloon and heat up the air whilst updrafts accelerate the balloon and cool the air adiabatically. The anticorrelation is not observed over the whole altitude range.





ACPD
10, 29971–29995, 2010



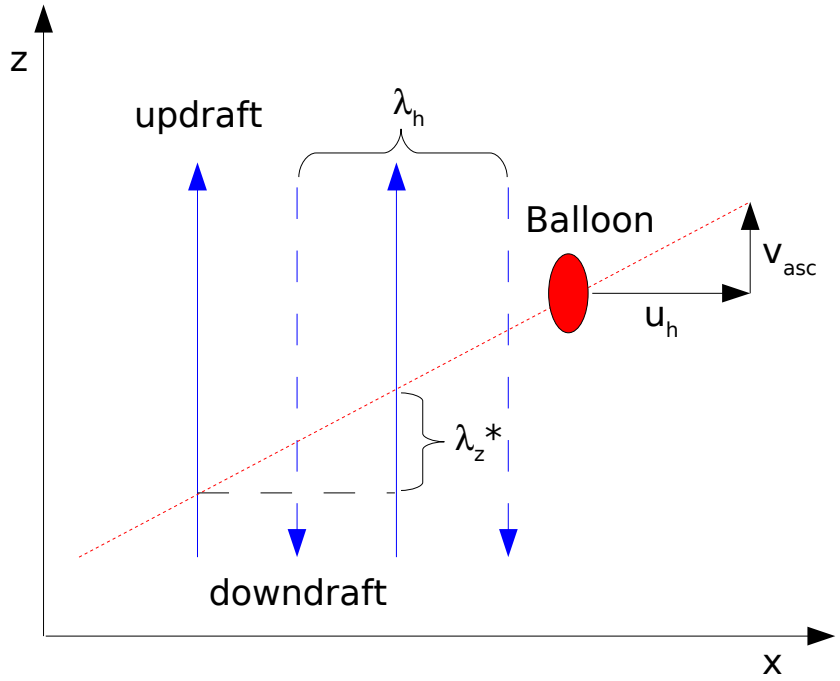


**Fig. 4.** Balloon ascending and traveling through the atmosphere crossing updraft and downdraft regions. The balloon has the horizontal speed $u_h$ and the vertical ascent rate $v_{asc}$. The wave displayed here has a horizontal wavelength $\lambda_h$ and the balloon experiences an apparent vertical wavelength of $\lambda_z^*$. We say apparent $\lambda_z^*$ since the real $\lambda_z = \infty$. Calculations with these assumptions are given in the text and lead to $\lambda_h = 11.7$ km.





ACPD
10, 29971–29995, 2010



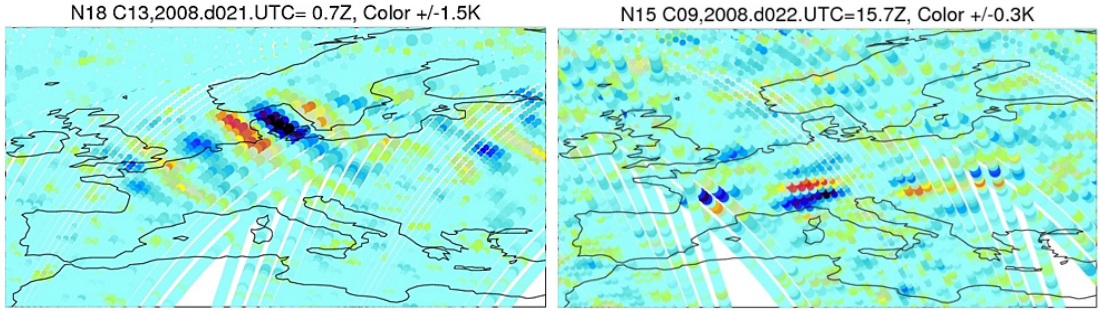


**Fig. 5.** AMSU radiances showing gravity waves over Europe. A picture of 21 January 2008 at 5 hPa on the left with horizontal wavelength of approx. 550 km and a picture of 22 January 2008 at 80 hPa with a wavelength of approx. 450 km.





ACPD
10, 29971–29995, 2010



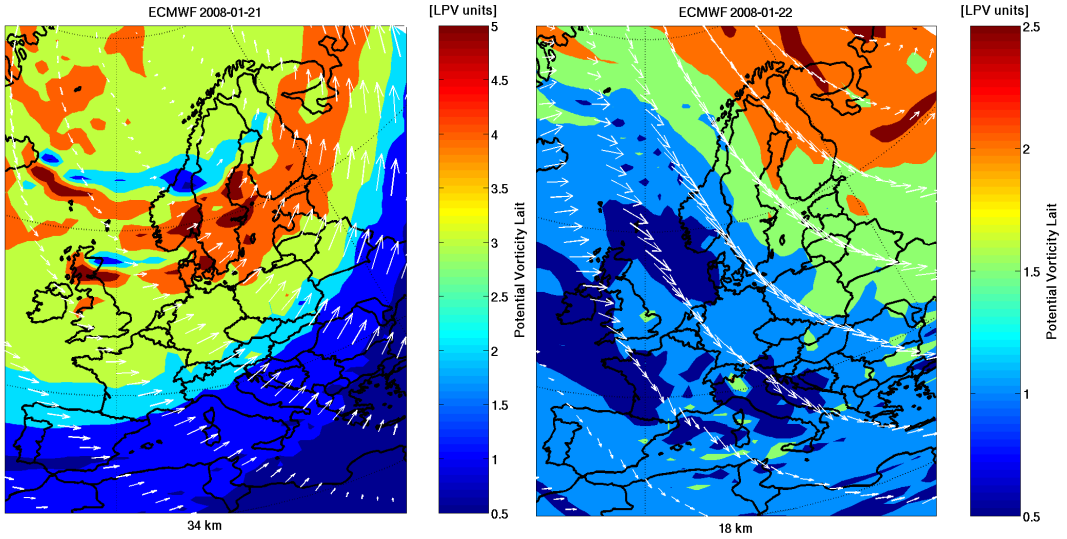


**Fig. 6.** ECMWF potential vorticity and horizontal wind direction (vectors) on same altitudes and times as in Fig. 5. The wind direction is perpendicular to the wave fronts shown in Fig. 5. The left figure is for 34 km altitude and the position of the vortex (red) corresponds well with the region of high wave amplitude. On the right figure at 18 km altitude the wind changes its direction after passing through the GW field over the Swiss Alps displayed in the corresponding right plot of Fig. 5.





ACPD
10, 29971–29995, 2010



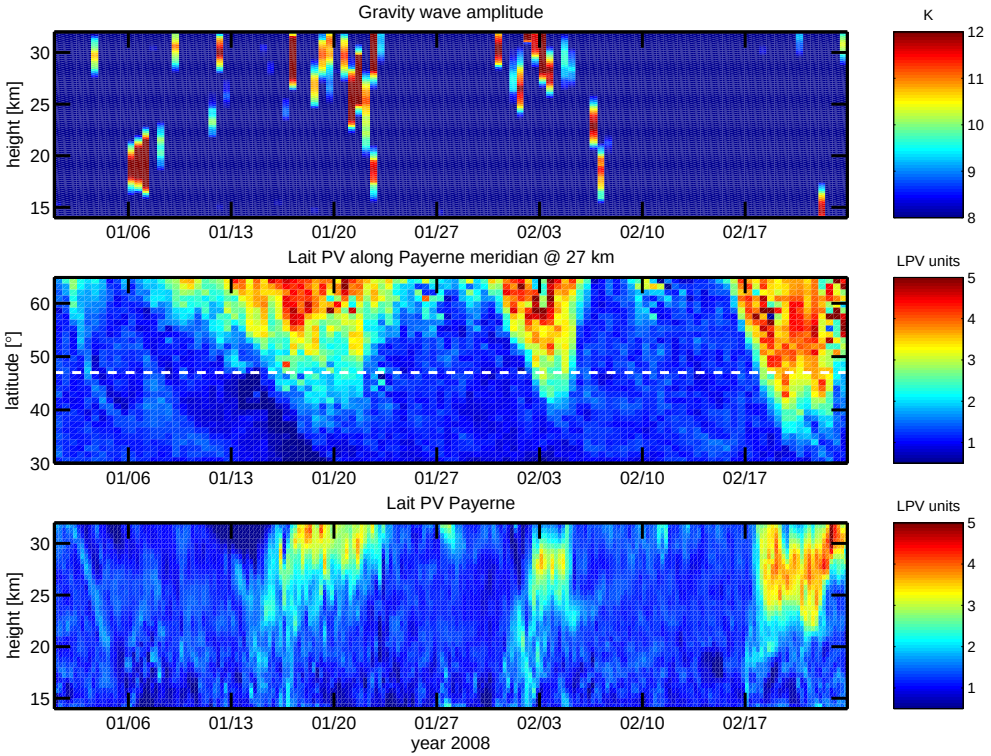


**Fig. 7.** Upper panel: Gravity wave amplitude calculated from radiosonde temperatures and averaged for all wave periods between 250 and 500 s. Middle panel: Time series of ECMWF Lait PV at 27 km along the Payerne meridian from 30° N to 65° N, the latitude of Payerne is marked by the white dashed line. The vortex edge can be identified as the light blue color. Lower panel: ECMWF Lait potential vorticity (LPV) for Payerne between 14 and 32 km altitude, LPV is high during the 3 SSW periods.





ACPD
10, 29971–29995, 2010

High gravity wave amplitudes during SSW

T. Flury et al.



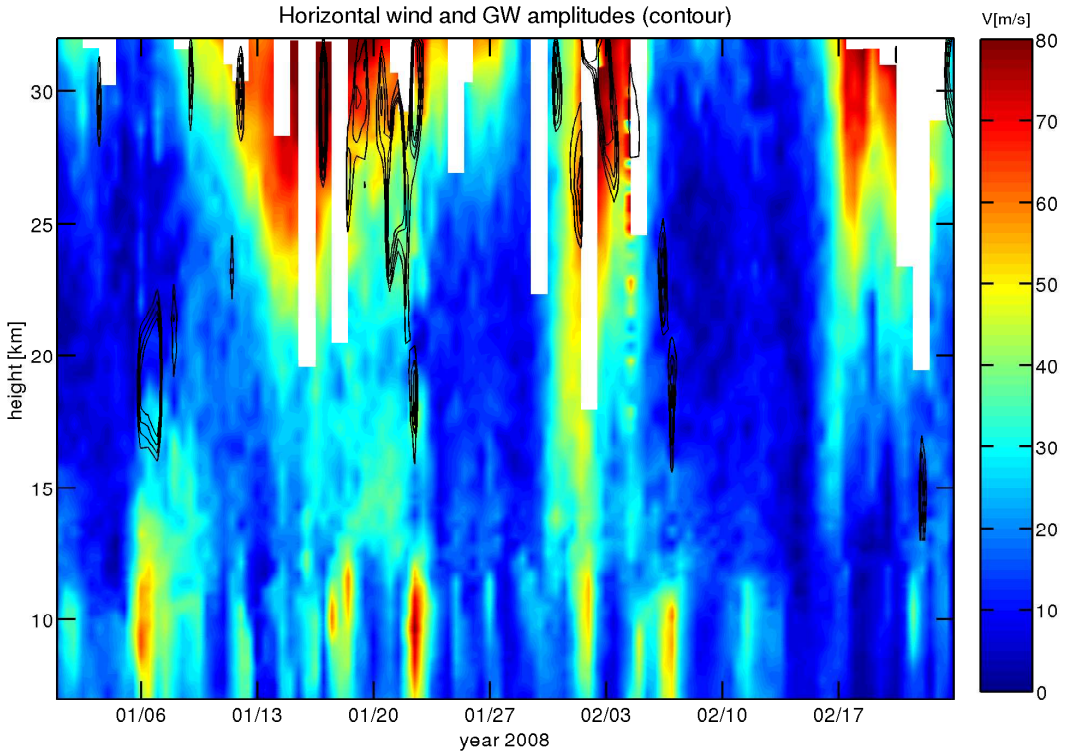


**Fig. 8.** Horizontal wind speed ($\sqrt{u^2+v^2}$, colors) measured by the radiosondes and the gravity wave amplitude (black, contour). The contours are plotted for amplitudes greater than 9 K (1 K distance of the contour lines). Occurrence of a strong tropopause jet (red color) is linked with GW activity in the lower stratosphere at 18 km and between 25 and 30 km altitude.





ACPD
10, 29971–29995, 2010



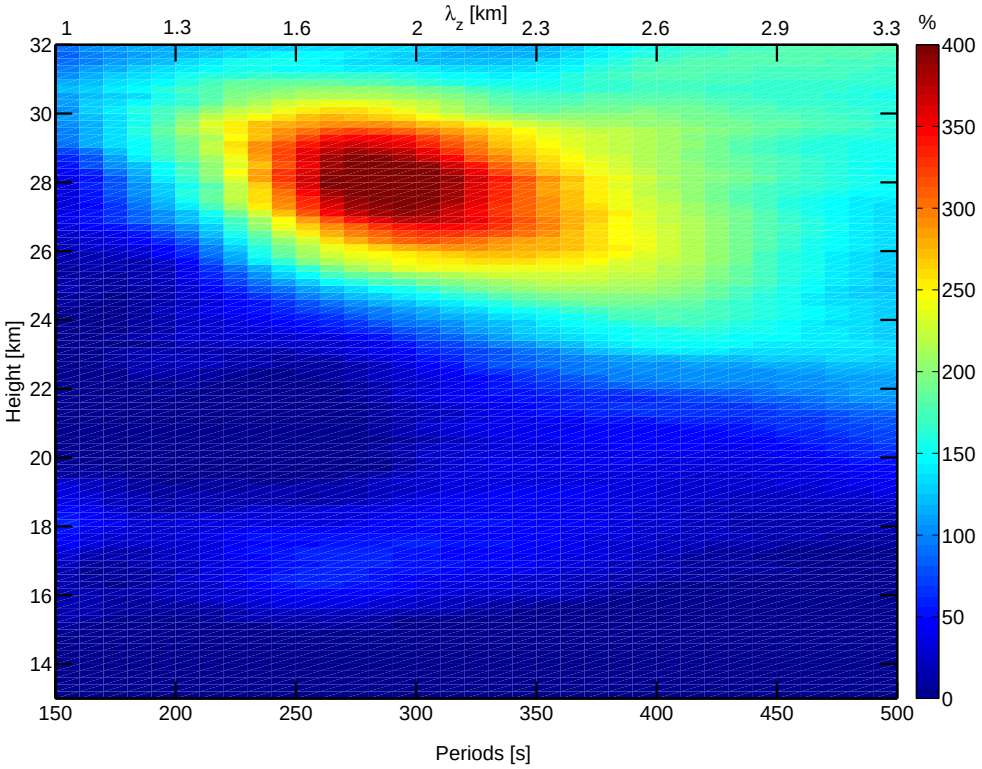


**Fig. 9.** Relative difference of the mean gravity wave amplitude (active period 18–22 January minus quiet period 23–30 January). The GW amplitude at the Brunt-Vaisala period of 300 s is 4 times increased during active conditions at altitudes from 25 to 30 km. The vertical wavelength is calculated assuming a mean ascent speed of the balloon of 6.5 m $s^{-1}$ and neglecting horizontal and temporal variations of the wave.





ACPD
10, 29971–29995, 2010